[Research Paper] 대한금속 · 재료학회지 (*Korean J. Met. Mater.*), Vol. 61, No. 5 (2023) pp.363-370
DOI: 10.3365/KJMM.2023.61.5.363

Bytizite Cu_3SbSe_3: Solid-State Synthesis and Thermoelectric Performance

Go-Eun Lee and Il-Ho Kim*

Department of Materials Science and Engineering, Korea National University of Transportation, Chungju 27469, Republic of Korea

Abstract: Bytizite (Cu_3SbSe_3) has attracted interest as a promising thermoelectric material because of its ultralow thermal conductivity; however, there are few experimental studies. This study investigated the optimal processing conditions for the synthesis of Cu_3SbSe_3 using mechanical alloying (MA) and hot pressing (HP). The MA powder exhibited an orthorhombic Cu_3SbSe_3 phase, which remained even after HP. However, secondary phases of permingeatite (Cu_3SbSe_4) and berzelianite ($Cu_{1.78}Se$) were also identified in the X-ray diffraction patterns. Thermal analysis revealed that the MA powder and HP compacts exhibited a large endothermic peak near 727 K, which corresponds to the melting point of Cu_3SbSe_3. Dense compacts with a relative density higher than 99% were obtained at HP temperatures above 573 K. Microstructural and elemental analyses confirmed the presence of the secondary phase Cu_3SbSe_4 in the matrix of Cu_3SbSe_3. However, the $Cu_{1.78}Se$ phase could not be observed. All specimens exhibited an electrical conductivity of (0.66–1.06) × 10^3 Sm^{-1}, a Seebeck coefficient of 324–376 μVK^{-1}, and a power factor of 0.09–0.11 $mWm^{-1}K^{-2}$ at 623 K. The thermal conductivity was lower than 0.7 $Wm^{-1}K^{-1}$ in the measured temperature range, mainly due to the phonon scattering caused by the lone-pair electrons of Sb. A dip in thermal conductivity was observed at 423 K, which was possibly caused by the order-disorder transition of bytizite. The dimensionless figure of merit ZT increased with increasing temperature, and the maximum ZT was 0.16 at 623 K.

(Received 6 January, 2023; Accepted 16 February, 2023)

Keywords: thermoelectric, bytizite, mechanical alloying, hot pressing

1. INTRODUCTION

With the increasing demand for sustainable energy and the rapid increase in the use of mobile devices, energy harvesting, which is the process of capturing/storing ambient energy (heat, light, vibration, etc.) and converting it into electrical energy, has received growing attention [1–4]. Thermoelectric conversion is a promising energy-harvesting technology because it can directly convert waste heat from vehicles, electronic devices, and human bodies into electrical energy. The energy conversion efficiency of a thermoelectric module is described by the figure of merit of the material, $Z = \alpha^2\sigma\kappa^{-1}$, where α, σ, and κ are the Seebeck coefficient, electrical conductivity, and thermal conductivity, respectively. The dimensionless figure of merit (ZT) multiplied by the figure of merit and absolute temperature (T) is used to compare thermoelectric materials that exhibit maximum performance at different operating temperatures. To achieve high efficiency, thermoelectric materials must have a high power factor ($\alpha^2\sigma$) and low thermal conductivity.

Ternary Cu-Sb-Se compounds containing earth-abundant and nontoxic elements are attracting attention as *p*-type semiconductors. Among them, Cu_3SbSe_3 (bytizite) is known to have anomalously low thermal conductivity because the electrostatic repulsion between the Sb 5s lone-pair electrons and neighboring chalcogen ions creates lattice anharmonicity [5]. In addition, using density functional theory (DFT), a predicted $ZT \approx 0.7$ at 600 K was reported, which indicates the potential of Cu_3SbSe_3 as a thermoelectric material [6]. However, there are limited experimental reports on its thermoelectric performance.

Several methods of synthesizing Cu_3SbSe_3 have been reported, such as bulk melting [7–9], nanocrystals prepared by the hot-injection method [10], and thin films by spray pyrolysis [11]. However, these methods are difficult to apply in devices because of their long processes or limited large-

- 이고은: 박사과정, 김일호: 교수
*Corresponding Author: Il-Ho Kim
[Tel: +82-10-5338-1582, E-mail: ihkim@ut.ac.kr]

scale production. In this study, mechanical alloying, which is suitable for large-scale production and a cost-effective method, was employed. In our previous study [12–14], ternary Cu-based chalcogenides were successfully synthesized via mechanical alloying (MA) and hot pressing (HP). Cu_3SbSe_3 bulks were prepared by the MA-HP process, and their phase synthesis (transformation) and thermoelectric properties were examined under MA-HP conditions.

2. EXPERIMENTAL

Raw elemental powders of Cu (<45 μm, purity 99.9%, Kojundo Chemical Lab., Japan), Sb (<150 μm, purity 99.999%, Kojundo Chemical Lab., Japan), and Se (<10 μm, purity 99.99%, Kojundo Chemical Lab., Japan) were weighed at stoichiometric ratios. MA was used to synthesize Cu_3SbSe_3 using a planetary ball mill (Pulverisette5, Fritsch, Germany), processed at 350 rpm for 6–24 h in a hardened steel jar with steel balls of 5 mm diameter at a ball-to-powder weight ratio of 20. The MA powders were loaded into a graphite mold (internal diameter of 10 mm) and consolidated by HP at 523–623 K for 2 h under a pressure of 70 MPa in a vacuum.

The phases of the MA powders and HP specimens were analyzed using X-ray diffraction (XRD; D2-Phaser, Bruker, Germany) with Cu K_α radiation (λ = 0.15405 nm), and the quantitative phase fractions and lattice constants were obtained using Rietveld refinement (TOPAS, Bruker, Germany). To identify the mass variation and phase transition, thermogravimetry and differential scanning calorimetry (TG-DSC; TG/DSC1, Mettler Toledo, USA) were carried out in the temperature range of 300–973 K at a heating rate of 5 $Kmin^{-1}$ in an Ar atmosphere. The microstructures of the polished and fractured surfaces of the HP specimens were observed using field-emission scanning electron microscopy (FESEM; JSM-7610F, Jeol, Japan), and their elemental compositions were analyzed using energy-dispersive spectroscopy (EDS; X-Max50, Oxford Instruments, UK).

The hot-pressed compacts were cut into rectangular shapes (3 mm × 3 mm × 9 mm) for Seebeck coefficient and electrical conductivity measurements, and into disc shapes (10 mm in diameter and 1 mm in thickness) for thermal diffusivity measurements. The Seebeck coefficient and electrical conductivity were simultaneously measured using a ZEM-3 (Advance Riko, Japan) system in He atmosphere. The thermal conductivity was estimated from the specific heat, density, and thermal diffusivity, measured using laser flash TC-9000H (Advance Riko, Japan) equipment in a vacuum. The thermoelectric power factor and figure of merit were evaluated at temperatures ranging from 323 to 623 K.

3. RESULTS AND DISCUSSION

Figure 1(a) presents the XRD patterns of the synthesized Cu_3SbSe_3 powders. The orthorhombic bytizite (Cu_3SbSe_3; space group *Pnma*) phase (PDF# 01-086-1751) was identified after MA for 6 h (MA350R6H). The secondary phase of tetragonal permingeatite (Cu_3SbSe_4; space group $I\bar{4}2\,m$) (PDF #01-085-0003) was observed, but the intensity of the diffraction peaks for Cu_3SbSe_4 did not decrease significantly, even with longer MA times. A quantitative analysis of the synthesized powders was conducted from the

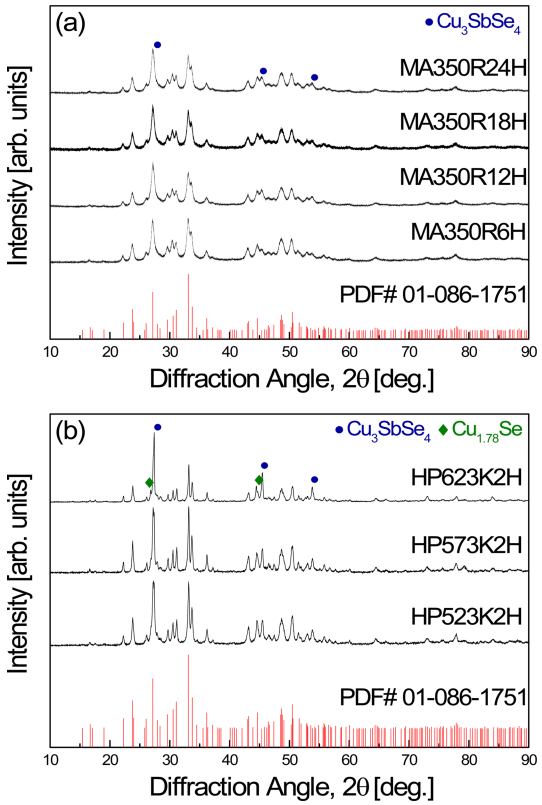

Fig. 1. XRD patterns of (a) synthesized powders and (b) sintered specimens of Cu_3SbSe_3.

Table 1. Quantitative analysis of synthesized powders and sintered specimens.

Specimen	Phase content (%)		
	Bytizite Cu_3SbSe_3	Permingeatite Cu_3SbSe_4	Berzelianite $Cu_{1.78}Se$
MA350R6H	88.3	11.7	-
MA350R12H	81.6	18.4	-
MA350R18H	85.1	14.9	-
MA350R24H	83.4	16.6	-
HP523K2H	78.5	16.0	5.5
HP573K2H	79.5	15.5	5.0
HP623K2H	65.1	26.8	8.1

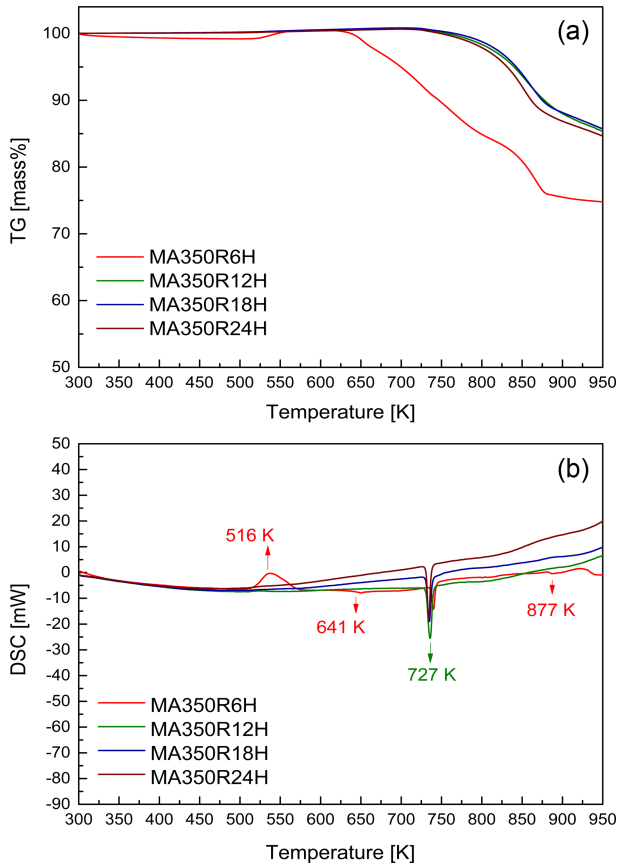

Fig. 2. Analyses of (a) TG and (b) DSC of the mechanically alloyed Cu_3SbSe_3.

XRD peaks, using Rietveld refinement, and the results are presented in Table 1. The MA time was adjusted from 6–24 h, and the Cu_3SbSe_4 phase was found to be 11.7–18.4%. In this study, further increasing the MA time did not change the phase composition, and a single Cu_3SbSe_3 phase could not be obtained by MA. Wei et al. [9] prepared Cu_3SbSe_3 using MA (450 rpm, 15 h)-HP (673 K, 1 h)-annealing (623 K, 5 d), but a secondary phase of Cu_3SbSe_4 was formed.

TG-DSC analyses of the MA powders were performed to confirm the phase transformation, and the results are shown in Figure 2. All of the MA powders showed a large endothermic peak at 727 K, which corresponds to the melting temperature of Cu_3SbSe_3. Wei et al. [9] determined the melting point of Cu_3SbSe_3 to be 730 K using DSC measurements. The melting point of Cu_3SbSe_4 is known to be approximately 733 K [15], similar to that of Cu_3SbSe_3; thus, the melting reaction peaks are not clear in Figure 2. The small exothermic and endothermic peaks of the MA350R6H specimen are possibly related to phase transitions resulting from mass loss, as shown in the TG curve (Figure 2a). Wei et al. [16] suggested that the exothermic peaks of $Cu_{3-x}SbSe_4$ synthesized by MA were associated with possible chemical reactions during the powder densification process. From the XRD and TG-DSC results, the optimal MA condition was determined to be 350 rpm for 18 h, and the effects of the HP conditions on the phase transformation and thermoelectric properties were examined.

Figure 1(b) shows the XRD patterns of the sintered specimens of Cu_3SbSe_3. The Cu_3SbSe_3 and Cu_3SbSe_4 phases in the MA powder remained even after HP, but a cubic berzelianite ($Cu_{1.78}Se$; space group $Fm\bar{3}m$) phase (PDF# 01-072-7490) also formed. Kirkham et al. [17] reported that approximately 10% of the secondary phases ($CuSbSe_2$ and Cu_2Se) were identified in the Cu_3SbSe_3 powder prepared by direct fusion annealing.

Liu et al. [18] prepared Cu_3SbSe_3 using self-propagating high-temperature synthesis (SHS) and spark plasma sintering (SPS) and detected the secondary phases of $Cu_{2-x}Se$ and $CuSbSe_2$. As shown in Table 1, the amount of Cu_3SbSe_3 phase increased slightly as the HP temperature increased from 523 to 573 K, but the Cu_3SbSe_4 and $Cu_{1.78}Se$ secondary phases increased significantly after HP at 623 K. The lattice constants of the specimens in Table 2 were a = 0.7985–0.8024 nm, b = 1.0655–1.0720 nm, and c = 0.6828–0.6873 nm, similar to those of Cu_3SbSe_3: ICDD standard diffraction data (PDF# 01-086-1751) with a = 0.7987 nm, b = 1.0614 nm, and c = 0.6837 nm.

Figure 3 shows the TG-DSC analyses of the hot-pressed Cu_3SbSe_3 specimens. The large endothermic peaks at 725–727 K were considered to be the melting points of Cu_3SbSe_3,

Table 2. Relative densities, lattice constants, and Lorenz numbers of Cu_3SbSe_3.

Specimen	Relative density [%]	Lattice constant [nm]			Lorenz number at 323 K [10^{-8} V^2K^{-2}]
		a	b	c	
MA350R18H	-	0.7993	1.0682	0.6835	-
HP523K2H	97.1	0.7985	1.0656	0.6833	1.618
HP573K2H	99.3	0.7986	1.0655	0.6828	1.579
HP623K2H	99.2	0.8024	1.0720	0.6873	1.583

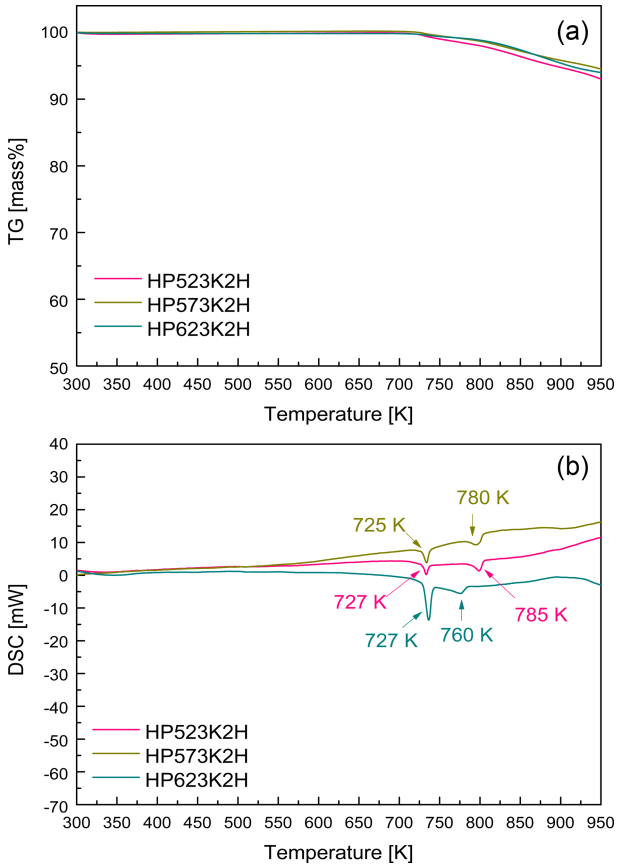

Fig. 3. Analyses of (a) TG and (b) DSC of the hot-pressed Cu_3SbSe_3.

as shown in Figure 2, and the small endothermic peaks at 760–785 K were interpreted to be the result of the phase change (decomposition) due to volatilization of the constituent elements. Because the melting point of $Cu_{2-x}Se$ detected in the XRD results was 1380 K [19], its reaction peaks did not appear in the measured temperature range.

Figure 4 shows the FESEM images of the polished and fractured surfaces of Cu_3SbSe_3. The HP523K2H specimen had a microstructure with many pores, which is consistent with the low sintered density shown in Table 2. The relative densities of the HP573K2H and HP623K2H specimens were higher than 99% of the theoretical density of Cu_3SbSe_3 (6.19 gcm^{-3}) [20]. The theoretical densities of the secondary phases Cu_3SbSe_4 and $Cu_{1.78}Se$ (or $Cu_{2-x}Se$) are known to be 5.86 gcm^{-3} [21] and 6.8 gcm^{-3} [22], respectively, but were excluded from the calculation of the relative density. The surface images in the backscattered electron mode exhibit differences in contrast, and the elemental analysis data of Cu_3SbSe_3 hot-pressed at 573 K for 2 h are displayed in Figure 5. The dark areas (A, B) and bright areas (C, D) were considered to be Cu_3SbSe_4 and Cu_3SbSe_3, respectively, which is in good agreement with the XRD results, while the $Cu_{1.78}Se$ phase detected in the XRD results was not found in the surface image.

Figure 6 shows the electrical conductivity of Cu_3SbSe_3 prepared using the MA-HP process. The electrical conductivity increased with increasing temperature, exhibiting nondegenerate semiconductor behavior, and increased with increasing HP temperature, resulting in an electrical conductivity of 1.06×10^3 Sm^{-1} at 623 K for HP623K2H. An increase in the sintering temperature can lead to increased carrier mobility, due to the reduction in interface density caused by grain growth and densification, which in turn increases the electrical conductivity [23, 24]. In addition, the presence of Cu_3SbSe_4 and $Cu_{1.78}Se$ phases, which have higher electrical conductivities than Cu_3SbSe_3, also possibly enhances the electrical conductivity [14, 25]. Liu et al. [18] reported that Cu_3SbSe_3 prepared by SHS-SPS exhibited an electrical conductivity of 1.6×10^3 Sm^{-1} at 653 K, which was higher than the value in their previous study, and the presence of $Cu_{2-x}Se$ possibly enhanced the electrical properties.

Therefore, the higher electrical conductivity of HP623K2H might be attributed to an increase in the fraction of secondary phases. Tyagi et al. [26] obtained an electrical conductivity of 1.4×10^3 Sm^{-1} at 550 K for Cu_3SbSe_3 prepared by melting-

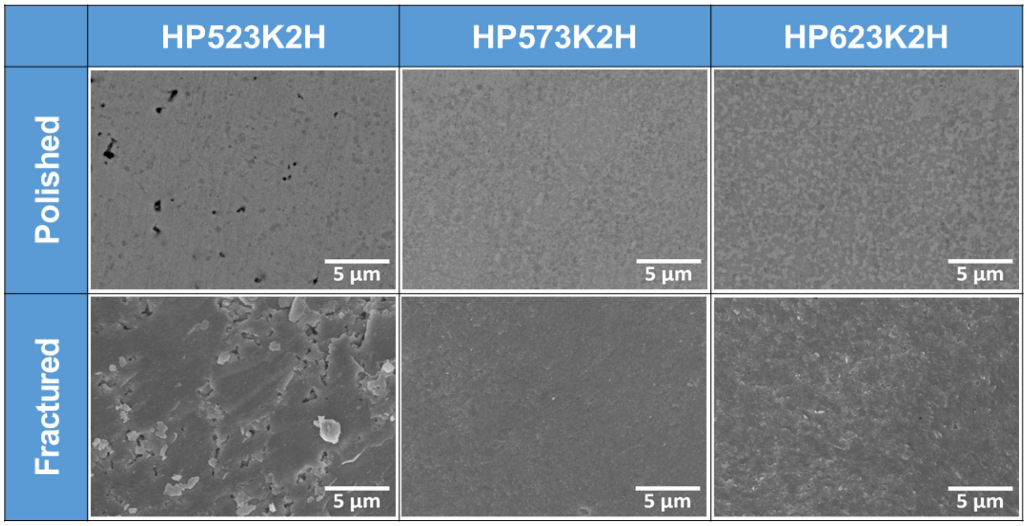

Fig. 4. FESEM images of the polished and fractured surfaces of Cu_3SbSe_3.

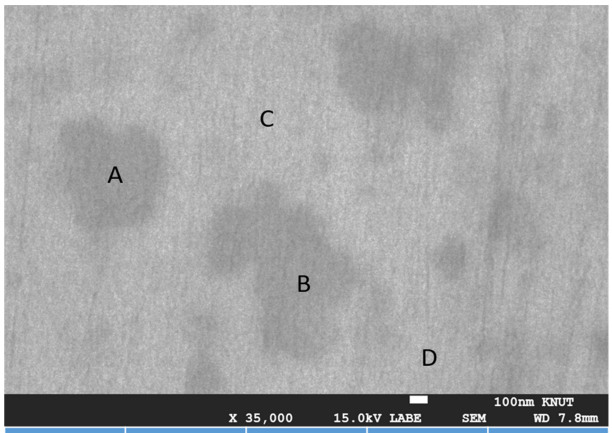

Region	A	B	C	D
Cu [at%]	41.68	40.82	46.00	46.00
Sb [at%]	14.03	13.91	13.76	12.94
Se [at%]	44.30	45.27	40.23	41.06

Fig. 5. Elemental analysis data of Cu_3SbSe_3 hot-pressed at 573 K for 2 h.

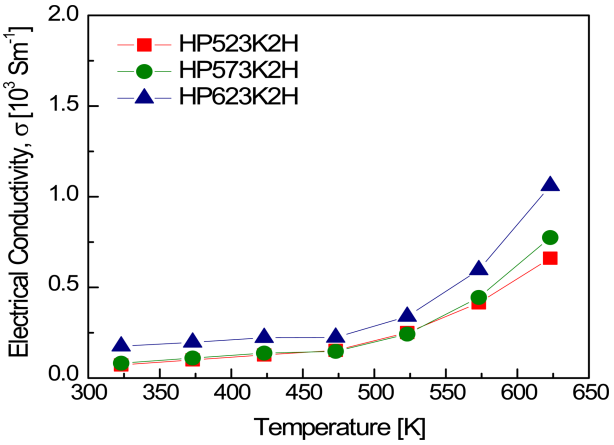

Fig. 6. Electrical conductivity of Cu_3SbSe_3 prepared by the MA-HP process.

SPS, and this low value was attributed to the low carrier concentration. Wei et al. [9] prepared Cu_3SbSe_3 using melting-annealing-HP and MA-HP-annealing, obtaining a carrier concentration of 10^{16}–10^{17} cm^3 and a carrier mobility of 10–20 $cm^2V^{-1}s^{-1}$ at room temperature.

Figure 7 shows the Seebeck coefficient of Cu_3SbSe_3 prepared with the MA-HP process. The Seebeck coefficient values were positive, indicating that *p*-type characteristics and holes were the major charge carriers. The Seebeck coefficient decreases with increasing temperature after exhibiting a maximum value, because of the intrinsic conduction by thermal excitation. As the HP temperature increased, the onset temperature of the intrinsic conduction shifted to a lower temperature. The Seebeck coefficient is inversely correlated with electrical conductivity; thus, the Seebeck coefficient decreases with increasing HP temperature. In this study, the Seebeck coefficient values for Cu_3SbSe_3 were 247–294 μVK^{-1} at 323 K and 324–359 μVK^{-1} at 623 K.

The power factor of Cu_3SbSe_3 prepared using the MA-HP process is shown in Figure 8. The power factor increased with temperature and HP temperature, and the maximum power factor was 0.09–0.11 $mWm^{-1}K^{-2}$ at 623 K. These

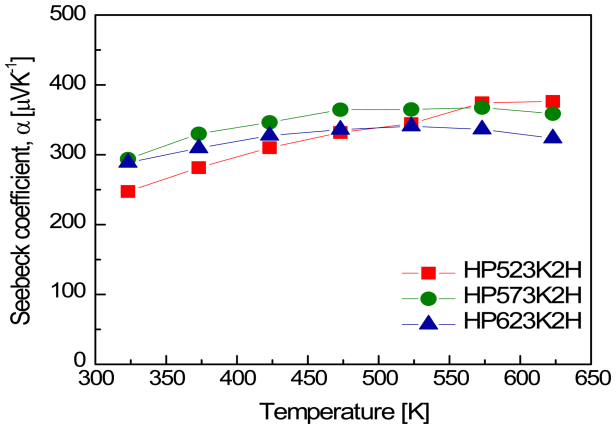

Fig. 7. Seebeck coefficient of Cu_3SbSe_3 obtained through the MA-HP process.

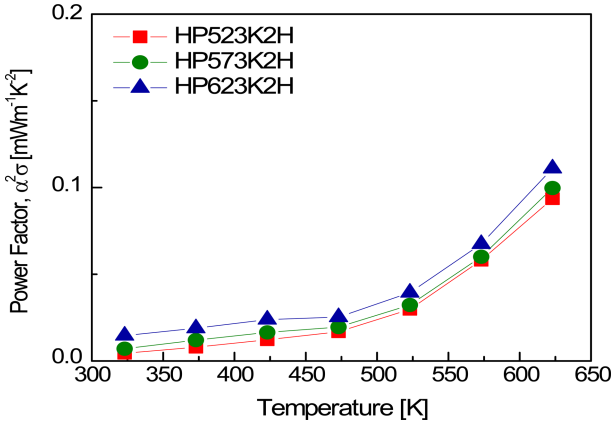

Fig. 8. Power factor of Cu_3SbSe_3 obtained through the MA-HP process.

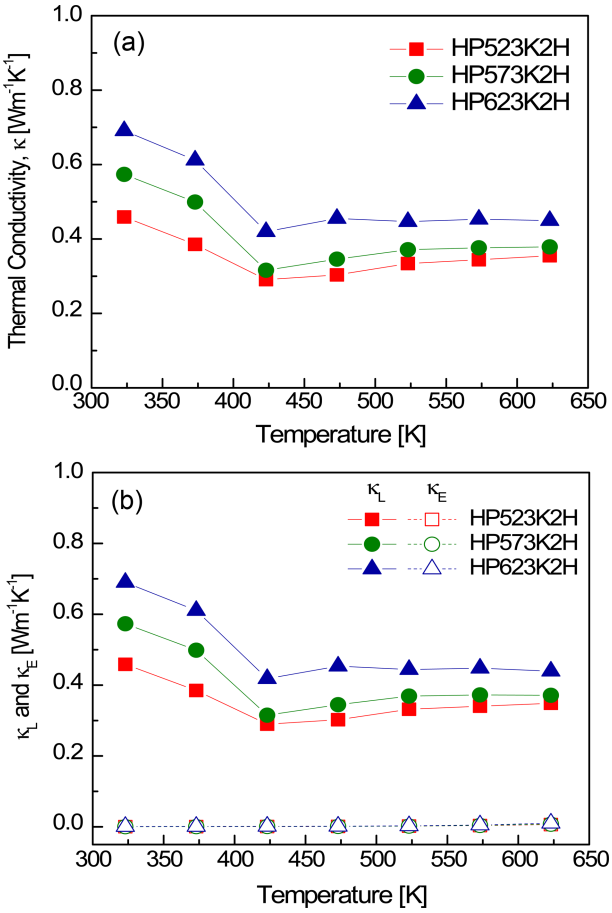

Fig. 9. Thermal conductivity of Cu_3SbSe_3 obtained through the MA-HP process; (a) total thermal conductivity and (b) lattice and electronic thermal conductivities.

values were similar to the 0.1 $mWm^{-1}K^{-2}$ of Cu_3SbSe_3 prepared by melting SPS [9]. The low power factor was mainly attributed to the low electrical conductivity caused by the low carrier concentration. Therefore, the electrical conductivity and power factor should be increased via doping.

Figure 9 presents the thermal conductivity of Cu_3SbSe_3 prepared with the MA-HP process. Thermal conductivity (κ) is attributed to lattice vibrations (κ_L: lattice thermal conductivity) and charge carrier transport (κ_E: electronic thermal conductivity), which can be separated using the Wiedemann-Franz law ($\kappa_E = L\sigma T$, L: temperature-dependent Lorenz number). The Lorenz number was calculated using the following equation: $L = 1.5 + \exp[-|\alpha|/116]$ [27], and the ranges of L were $(1.58–1.62) \times 10^{-8}$ V^2K^{-2} at 323 K and $(1.54–1.56) \times 10^{-8}$ V^2K^{-2} at 623 K, indicating that Cu_3SbSe_3 is a nondegenerate semiconductor, as demonstrated by the temperature dependence of electrical conductivity. Theoretically, the Lorenz number is in the range of $(1.45–2.44) \times 10^{-8}$ V^2K^{-2} [28], and smaller values indicate nondegenerate semiconductor behavior. The thermal conductivity decreases rapidly at 423 K and then increases slightly. Kirkham et al. [17] found an order-disorder transition in Cu_3SbSe_3 at 373–448 K because of the mobile Cu atoms, and a change in the slope from negative to positive at the transition temperature was confirmed by thermal conductivity measurements. Similarly, significant changes in the thermal conductivity and specific heat of Cu_3SbSe_3 at 373–450 K have been reported [9, 18, 26, 29]. The thermal conductivity values of all specimens were less than 0.7 $Wm^{-1}K^{-1}$ in the temperature range of 323–623 K, and the minimum thermal conductivity was 0.29–0.42 $Wm^{-1}K^{-1}$ at 423 K. The

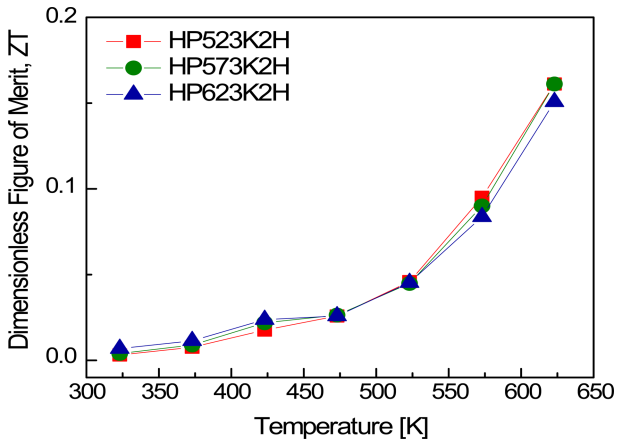

Fig. 10. Dimensionless figure of merit of Cu_3SbSe_3 obtained with the MA-HP process.

thermal conductivity was almost temperature-independent after the order-disorder transition. According to the report by Skoug et al. [5], in the group A^V-chalcogenide compounds, the electrostatic repulsion between the Sb 5s lone-pair electrons and neighboring chalcogen ions causes lattice anharmonicity, and their strength is determined by the morphology of the lone-pair orbital and the coordination number of the group A^V atom. Thus, Cu_3SbSe_3 with the largest Se-Sb-Se bond angle (99.42°) exhibits temperature-independent behavior and the lowest lattice thermal conductivity (0.49 $Wm^{-1}K^{-1}$ at 300 K).

Figure 10 shows the dimensionless figure of merit (*ZT*) of Cu_3SbSe_3 prepared via the MA-HP process. The *ZT* values increased with increasing temperature, and the maximum *ZT* value was 0.16 at 623 K. Tyagi et al. [26] obtained $ZT < 0.1$ in the temperature range of 300–600 K for Cu_3SbSe_3 prepared by melting-SPS, and Wei et al. [9] achieved $ZT = 0.25$ at 650 K for Cu_3SbSe_3 prepared by both melting-annealing-HP and MA-HP-annealing. Liu et al. [18] reported $ZT = 0.42$ at 653 K for Cu_3SbSe_3 prepared by SHS-SPS. Although intrinsic Cu_3SbSe_3 exhibited a low ZT value, Cu_3SbSe_3 could be a potential thermoelectric material because of its large Seebeck coefficient and low thermal conductivity, and its thermoelectric performance is expected to be enhanced by stabilizing the bytizite phase and increasing the power factor through doping.

Figure 10 shows the dimensionless figure of merit (*ZT*) of Cu_3SbSe_3 prepared via the MA-HP process. The *ZT* values increased with increasing temperature, and the maximum *ZT* value was 0.16 at 623 K. Tyagi et al. [26] obtained $ZT < 0.1$ in the temperature range of 300–600 K for Cu_3SbSe_3 prepared by melting-SPS, and Wei et al. [9] achieved $ZT = 0.25$ at 650 K for Cu_3SbSe_3 prepared by both melting-annealing-HP and MA-HP-annealing. Liu et al. [18] reported $ZT = 0.42$ at 653 K for Cu_3SbSe_3 prepared by SHS-SPS. Although intrinsic Cu_3SbSe_3 exhibited a low ZT value, Cu_3SbSe_3 could be a potential thermoelectric material because of its large Seebeck coefficient and low thermal conductivity, and its thermoelectric performance is expected to be enhanced by stabilizing the bytizite phase and increasing the power factor through doping.

4. CONCLUSIONS

Orthorhombic bytizite Cu_3SbSe_3 was synthesized using MA-HP without post-annealing, but secondary phases of tetragonal permingeatite Cu_3SbSe_4 and cubic berzelianite $Cu_{1.78}Se$ were formed. From the XRD and TG-DSC results, the optimal MA condition was determined to be 350 rpm for 18 h. Dense specimens close to the theoretical density were obtained at HP temperatures above 573 K. All specimens showed *p*-type conduction and nondegenerate behavior. With increasing HP temperature, the electrical conductivity increased, while the Seebeck coefficient decreased. All specimens exhibited low thermal conductivity values of <0.7 $Wm^{-1}K^{-1}$, and the minimum values were 0.29–0.42 $Wm^{-1}K^{-1}$ at 423 K. The largest power factor of 0.11 $mWm^{-1}K^{-2}$ and the maximum *ZT* of 0.16 were achieved at 623 K. The *ZT* value of Cu_3SbSe_3 was lower than that of other promising Cu-chalcogenides; nevertheless, it is expected that the thermoelectric performance can be improved by increasing the power factor via doping, because it has a moderate Seebeck coefficient and ultralow thermal conductivity.

Acknowledgment

This study was supported by the Basic Science Research Capacity Enhancement Project (National Research Facilities and Equipment Center) through the Korea Basic Science Institute funded by the Ministry of Education (Grant No. 2019R1A6C1010047).

REFERENCES

1. I. J. Lee, S. B. Park, S. C. Ur, K. W. Jang, and I. H. Kim, *Korean J. Met. Mater.* **57**, 264 (2019).
2. S. H. Choe, Y. S. Kim, J. Y. Choi, Y. J. Park, B. C. Cha, Y. M. Kong, and D. Kim, *Korean J. Met. Mater.* **57**, 506 (2019).
3. Y. J. Jang, H. J. Shin, S. J. Wi, H. N. Kim, G. S. Lee, and J. Ahn, *Korean J. Met. Mater.* **57**, 124 (2019).
4. C. Lee, K. Bang, D. Hong, and H. M. Lee, *Korean J. Met. Mater.* **57**, 1 (2019).
5. E. J. Skoug and D. T. Morelli, *Phys. Rev. Lett.* **107**, 235901 (2011).
6. C. Sevik and T. Čağin, *J. Appl. Phys.* **109**, 1 (2011).
7. P. W. Majsztrik, M. Kirkham, V. Garcia-Negron, E. Lara-Curzio, E. J. Skoug, and D. T. Morelli, *J. Mater. Sci.* **48**, 2188 (2013).
8. K. Tyagi, B. Gahtori, S. Bathula, V. Toutam, S. Sharma, N. K. Singh, and A. Dhar, *Appl. Phys. Lett.* **105**, 261902 (2014).
9. T. R. Wei, C. F. Wu, W. Sun, Y. Pan, and J. F. Li, *RSC Adv.* **5**, 42848 (2015).
10. Y. Liu, J. Yang, E. Gu, T. Cao, Z. Su, L. Jiang, C. Yan, X. Hao, F. Liu, and Y. Liu, *J. Mater. Chem. A* **2**, 6363 (2014).
11. A. A. Akl, I. M. El Radaf, and A. S. Hassanien, *Optik* **227**, 165837 (2021).
12. S. Y. Kim, S. G. Kwak, J. H. Pi, G. E. Lee, and I. H. Kim, *J. Electron. Mater.* **48**, 1857 (2019).
13. G. E. Lee, J. H. Pi, and I. H. Kim, *J. Electron. Mater.* **49**, 2781 (2020).
14. G. E. Lee and I. H. Kim, *Materials* **14**, 1116 (2021).
15. E. J. Skoug, J. D. Cain, P. Majsztrik, M. Kirkham, E. Lara-Curzio, and D. T. Morelli, *Sci. Adv. Mater.* **3**, 602 (2011).
16. T. R. Wei, F. Li, and J. F. Li, *J. Electron. Mater.* **43**, 2229 (2014).
17. M. Kirkham, P. Majsztrik, E. Skoug, D. Morelli, H. Wang, W. D. Porter, E. A. Payzant, and E. Lara-Curzio, *J. Mater. Res.* **26**, 2001 (2011).
18. R. Liu, G. Ren, X. Tan, Y. Lin, and C. Nan, *Energies* **9**, 816 (2016).
19. V. M. Glazov, A. S. Pashinkin, and V. A. Fedorov, *Inorg. Mater.* **36**, 641 (2000).
20. A. Jain, S. P. Ong, G. Hautier, W. Chen, W. D. Richards, S. Dacek, S. Cholia, D. Gunter, D. Skinner, G. Ceder, and K. A. Persson, *APL Mater.* **1**, 011002 (2013).
21. Y. Li, X. Qin, X. Yang, Y. Liu, J. Zhang, Y. Dou, C. Song, and H. Xin, *J. Mater. Chem. C* **3**, 7045 (2015).
22. D. Shi, Z. Geng, and K. H. Lam, *Energies* **12**, 401 (2019).
23. J. Seo, K. Park, D. Lee, and C. Lee, *Mater. Sci. Eng. B* **49**, 247 (1997).
24. J. S. Son, M. K. Choi, M. K. Han, K. Park, J. Y. Kim, S. J. Lim, M. Oh, Y. Kuk, C. Park, S. J. Kim, and T. Hyeon, *Nano Lett.* **12**, 640 (2012).
25. L. Yang, Z. G. Chen, G. Han, M. Hong, and J. Zou, *Acta Mater.* **113**, 140 (2016).
26. K. Tyagi, B. Gahtori, S. Bathula, A. K. Srivastava, A. K. Shukla, S. Auluck, and A. Dhar, *J. Mater. Chem. A* **2**, 15829 (2014).
27. H. S. Kim, Z. M. Gibbs, Y. Tang, H. Wang, and G. J. Snyder, *APL Mater.* **3**, 041506 (2015).
28. E. Flage-Larsen and Ø. Prytz, *Appl. Phys. Lett.* **99**, 202108 (2011).
29. K. Samanta, N. Gupta, H. Kaur, L. Sharma, S. Dogra Pandey, J. Singh, T. D. Senguttuvan, N. Dilawar Sharma, and A. K. Bandyopadhyay, *Mater. Chem. Phys.* **151**, 99 (2015).